INTERNATIONAL JOURNAL FOR NUMERICAL METHODS IN FLUIDS, VOL. 15, 545–569 (1992)

FLOW FIELD MODELLING NEAR A WELL WITH A CONDUCTIVE FRACTURE

Y. C. LI AND N. C. HUANG

Department of Aerospace and Mechanical Engineering, University of Notre Dame, Notre Dame, IN 46556, U.S.A.

SUMMARY

In the technology of oil recovery the oil production rate can be increased by generation of a vertical sand-filld conductive fracture on the wall of the well. Oil diffuses through the conductive fracture to the well. In this paper the seepage flow and isothermal deformation fields in both the formation and fracture and the oil production rate at the well are studied by modelling the formation as an infinite poroelastic medium saturated with a one-phase compressible fluid. The fracture is treated as a one-dimensional poroelastic medium. Darcy flows are considered in both the formation and fracture. The plane strain condition is imposed. Our solution is obtained numerically by a finite element method based on a variational principle. The accuracy of the analysis is studied by comparison of the numerical solutions of some problems with their analytical solutions. Since we are dealing with the transient flow problem of an infinite region, an extrapolation technique is employed to find the finite element solution. The production rate of a well with the conductive fracture is compared with that of a well without the conductive fracture.

KEY WORDS Oil recovery Porous medium Conductive fracture Finite element method

INTRODUCTION

Analysis of the flow field in an oil-bearing formation near a production well is important in the study of hydraulic fracture growth and in the determination of the relationship between the oil production rate and the applied pressure in the well during oil recovery. The simplest problem of primary oil recovery deals with a single well at the centre of a cylindrical porous medium. If the deformation of the medium is ignored, the flow field in the formation is governed by a diffusion equation. Its analytical solution has been used to predict the oil production rate and the flow field in the reservoir. When the permeability of the reservoir is low, the hydraulic fracture technique can be used to increase the production rate. In this technique a high pressure is applied to the production well through the injected fluid to generate a crack. The injected fluid carries highly permeable material, e.g. sand, which displaces into the crack with the fluid. As the applied pressure is removed, the sand remains in the crack to form a sand band which keeps the crack open. The production rate can be raised owing to the increase in diffusive area from the conductive crack.

In the following we shall consider the pressure transient behaviour of a hydraulically fractured well. Our model consists of a fully penetrating vertical well located at the centre of a fully penetrating vertical fracture. At present, several exact and approximate analytical solutions can be found in the literature for determination of the effect of the conductive fracture on well

0271–2091/92/170545–25$17.50

Received February 1991
Revised March 1992

performance and transient pressure behaviour. In these studies the coupling effect of the deformation of the medium and the flow field in the medium is neglected. Gringarten *et al.*[1] presented a type-curve analysis and found three basic solutions: (i) the infinite fracture conductivity solution associated with the uniformly distributed applied pressure along a vertical fracture, (ii) the uniform flux solution for a vertical fracture and (iii) the uniform flux solution for a horizontal fracture. Kucuk[2] and Kucuk and Brigham[3] considered the problem of elliptical flow in an infinite and undeformable reservoir with an elliptical inner boundary. The initial pressure in the reservoir is uniform and the inner boundary of the medium is subjected to a prescribed, uniformly distributed pressure. Elliptical co-ordinates and the Laplace transform technique are used in their analysis. Their solution of pressure distribution is expressed as an infinite series of inverse Laplace transforms of Mathieu functions. Production rates are found for different prescribed constant pressures under different times. For the case of finite fracture conductivity a solution has been obtained by Cinco-Ley *et al.*[4] In their solution the crack is assumed to be rectangular with an impermeable crack tip. The effect of crack width is ignored when the pressure diffusion in the medium is studied. The flow flux through the well wall is also neglected. Hence all the flow into the well stems from the conductive fracture. The solutions of the pore pressures in the medium and conductive fracture can be expressed as integral equations using Green and source functions. These integrals include the flow flux density across the crack surface. The integration is taken along the crack line and with respect to time. With the use of the continuity conditions of pressure and flow flux density on the crack surface, the two solutions can be combined into a Fredholm integral equation where the only unknown is the flow flux density. This integral equation is then solved by discretization of the flow flux density in time and space. In this solution the flux density is assumed to have a stepwise distribution in time and space.

In this paper, problems of determination of deformation and flow fields in an infinite medium containing a single production well with/without a conductive crack will be considered. The theory of linear and isotropic poroelasticity given by Biot[5] for modelling a fluid-saturated porous rock is employed in the analysis. The variational principle based on Biot's field equations is presented and the finite element method for pressure–deformation coupled problems given by Huang *et al.*[6] is used for simulation of the oil flow field. Useful information is obtained for prediction of oil production rate, flow field and deformation field near the production well.

GOVERNING EQUATIONS AND VARIATIONAL PRINCIPLE

For the porous medium

Let us consider a homogeneous and isotropic poroelastic medium saturated with a single phase compressible fluid and subjected to a small deformation. The governing equations for a three-dimensional isothermal medium are given by Biot[5] as follows:

strain–displacement relations,

$$\varepsilon_{ij}=\tfrac{1}{2}(u_{i,j}+u_{j,i}); \tag{1}$$

equations of equilibrium,

$$\sigma_{ij,j}=0; \tag{2}$$

constitutive relations,

$$\sigma_{ij}+\lambda p\delta_{ij}=H_{ijkl}\varepsilon_{kl}, \tag{3}$$

$$\Theta=\lambda\varepsilon_{kk}+cp; \tag{4}$$

equation of conservation of mass,

$$v_{i,i}+\dot{\Theta}=0; \tag{5}$$

Darcy's law,

$$v_i=-K p_{,i}; \tag{6}$$

where u_i is the displacement vector, ε_{ij} is the strain tensor, σ_{ij} is the stress tensor, p is the change in pore pressure above the confining pressure, v_i is the flow velocity of the liquid in the porous medium, Θ is the increase in fluid content as the result of a change in pore size, K is the permeability coefficient, c is the compressibility of the fluid, λ is the poroelastic constant, H_{ijkl} is the stress–strain relation tensor, δ_{ij} is the Kronecker delta, $()_{,i}=\partial(\ )/\partial x_i$ and $\dot{(\ )}=\partial(\ )/\partial t$. Note that the body forces of the medium and fluid are ignored. The permeability coefficient K is related to the permeability k by

$$K=k/(\phi\mu), \tag{7}$$

where ϕ is the porosity of the medium and μ is the dynamic viscosity of the fluid. For an isotropic medium the stress–strain relation tensor H_{ijkl} can be expressed by

$$H_{ijkl}=2G\left(\delta_{ik}\delta_{jl}+\frac{\nu}{1-2\nu}\delta_{ij}\delta_{kl}\right), \tag{8}$$

where G is the shear modulus and ν is Poisson's ratio. Equations (4)–(6) can be combined into

$$-Kp_{,ii}+\lambda\dot{\varepsilon}_{ii}+c\dot{p}=0. \tag{9}$$

Note that if $\lambda=0$, equation (9) reduces to a typical diffusion equation of the pore pressure.

The porous medium occupies a volume V with a surface S. The boundary conditions are

$$u_i=u_i^* \quad \text{on } S_u, \tag{10}$$

$$\sigma_{ij}n_j=P_i^* \quad \text{on } S_\sigma, \tag{11}$$

$$p=p^* \quad \text{on } S_p, \tag{12}$$

$$v_i n_i=V_n^* \quad \text{on } S_v, \tag{13}$$

where $S_u+S_\sigma=S_p+S_v=S$ and n_i is the component of the outward unit normal to the surface. All the starred quantities are the corresponding prescribed quantities on the boundaries. They are regarded as time-dependent. Assuming that the boundary conditions are applied gradually, the initial conditions at $t=0^+$ are

$$u_i(x_1, x_2, x_3; 0^+)=0, \tag{14}$$

$$\Theta(x_1, x_2, x_3; 0^+)=0, \tag{15}$$

$$p(x_1, x_2, x_3; 0^+)=0. \tag{16}$$

Our variational principle is established on the basis of the Laplace-transformed quantities. In the following we shall denote the Laplace-transformed quantities by an overbar. Let us consider the following functional of the Laplace-transformed quantities:

$$\Phi=\int_v\left(\tfrac{1}{2}H_{ijkl}\bar{\varepsilon}_{ij}\bar{\varepsilon}_{kl}+\lambda\bar{p}\bar{\varepsilon}_{ii}-\frac{K}{2s}\bar{p}_{,i}\bar{p}_{,i}-\frac{c}{2}\bar{p}^2\right)dV-\int_{S_\sigma}\bar{P}_i^*\bar{u}_i\,dS-\int_{S_v}\frac{1}{s}\bar{V}_n^*\bar{p}\,dS, \tag{17}$$

where s is the variable of Laplace transformation. It can be shown that among all $\bar{u}_i$ and $\bar{p}$ satisfying the Laplace-transformed strain–displacement relation (1) and boundary conditions

(10) and (12), the actual solution of $\bar{u}_i$ and $\bar{p}$ would make Φ stationary, i.e. the first variation of Φ satisfies

$$\delta\Phi = 0. \tag{18}$$

For the plane strain problem the foregoing governing equations and variational functional still hold, but all material constants should be replaced by the corresponding quantities in the plane strain case.[6] Also, the volume integrals and surface integrals should be replaced by the area integrals and contour integrals respectively.

For the fracture

When the pressure in the injected fluid is higher than the *in situ* stress, an initial fracture can be generated. The fluid in the fracture contains sand. As the applied pressure is removed, the sand carried by the fluid will remain in the formation to form a conductive fracture. In the following we assume that this procedure is completed in a sufficiently short time. Therefore a problem with non-zero initial displacement and pressure fields can be formulated.

Let us consider a plane strain problem in a Cartesian co-ordinate frame with the origin at the well-bore. The initial fracture is located on the x_1-axis from $x_1 = -a$ to $x_1 = a$. The governing equations (1)–(6) still hold in the conductive fracture, but all material constants are denoted by adding a subscript 'f' referring to the constants of the fracture. Since the crack is narrow, the flow in the fracture can be considered to be one-dimensional and the strain components ε_{11} and ε_{12} can be neglected in comparison with the transverse normal strain ε_{22}. Correspondingly, the stress components σ_{11} and σ_{12} can also be neglected. After integration of equations (3)–(6) through the width of the crack it is found that

$$\sigma_{22} + \lambda_f p = E_f \varepsilon_{22}, \tag{19}$$

$$\Theta = \lambda_f \varepsilon_{22} + c_f p, \tag{20}$$

$$v_{1,1}\delta + \dot{\Theta}\delta + 2v_n = 0, \tag{21}$$

$$v_1 = -K_f p_{,1}, \tag{22}$$

where v_n is the leak-off velocity, which is positive for the outward flow of fluid into the medium, δ is the crack-opening displacement and E_f is Young's modulus of the sand-filled conductive fracture. Equations (20)–(22) can be combined into

$$\delta(-K_f p_{,11} + \lambda_f \dot{\varepsilon}_{22} + c_f \dot{p}) + 2v_n = 0. \tag{23}$$

If the upper half-plane is taken into consideration, the traction on the fracture surface is $T_2 = -\sigma_{22}$. Since the change in δ is small, the value of δ can be approximated by the initial crack-opening displacement δ_0. The transverse strain can be expressed by

$$\varepsilon_{22} = \frac{\delta - \delta_0}{\delta_0}. \tag{24}$$

Thus, equations (19) and (23) become

$$-T_2 + \lambda_f p = E_f \varepsilon_{22}, \tag{25}$$

$$\delta_0(-K_f p_{,11} + c_f \dot{p}) + \lambda_f \dot{\delta} + 2v_n = 0. \tag{26}$$

The leak-off velocity v_n can be expressed as

$$v_n = -K \left.\frac{\partial p}{\partial x_2}\right|_{x_2 = 0}. \tag{27}$$

The boundary conditions are

$$K_f \frac{\partial}{\partial x_1} p(a^-, 0; t) = K \frac{\partial}{\partial x_1} p(a^+, 0; t) \quad \text{for } x_1 = a \tag{28}$$

and either

$$p(r_w, 0; t) = p_w \quad \text{for } x_1 = r_w \tag{29}$$

when the applied pressure at the well is prescribed or

$$-2K_f \delta_0 \frac{\partial}{\partial x_1} p(r_w, 0; t) - \int_0^{2\pi} K \frac{\partial}{\partial n} p(r_w, \theta; t) r_w \mathrm{d}\theta = q_w \quad \text{for } x_1 = r_w \tag{30}$$

when the production rate is prescribed, where θ is the polar angle. In equations (27)–(30) r_w is the radius of the well, p_w is the prescribed applied pressure at the well and q_w is the prescribed production rate per unit height of the formation. On the left-hand side of equation (30) the integral term denotes the flow rate across the well wall and the other term is the flow rate from the conductive fracture.

COMPUTATIONAL SCHEMES

In our finite element method the variational equations (17) and (18) are converted to a set of linear algebraic equations. After inverse Laplace transformation these equations include time derivatives of nodal displacements and pore pressure. These derivatives will be evaluated by two-step backward finite difference expressions. The flow equation (26) for the fracture can be partitioned into a set of finite difference equations which are coupled with the set of finite element equations. The two sets of equations will be solved simultaneously.

For the finite elements in the immediate vicinity of the crack tip, as a result of the inverse square root singularity in stress and strain components, the interpolation functions for the displacement components take a singular form suggested by Rice and Tracey[7]. For other elements the values of displacements in elements are expressed by a regular four-node isoparametric interpolation of their nodal values. The interpolation formula for the pore pressure also takes the regular from for all elements in the entire region.

For any transient and infinite region problem the finite element solution with the infinite region replaced by a finite region is accurate only for sufficiently small time. In this paper the numerical solutions for large time will be derived by an extrapolation method. In this technique we first use the finite element method to find a group of solutions for the problems in the finite regions. Let R be the radius of each finite region. Set $\xi = 1/R^2$. The calculated quantities can be treated as functions of ξ. The solution for the infinite region problem at any time can be extrapolated at $\xi = 0$. Let z stand for some kind of solutions for a finite region of radius R. The extrapolation function is chosen to have the form

$$z = a_1 \xi^3 + a_2 \xi^2 + a_3, \tag{31}$$

where a_1, a_2 and a_3 are constant coefficients. This extrapolation function has a feature that the derivative $\mathrm{d}z/\mathrm{d}\xi$ is equal to zero at $\xi = 0$. It can be shown by the Laplace transform technique that in the problem of radial pressure diffusion the quantity $R^3 \mathrm{d}p/\mathrm{d}R$ has a zero limiting value when R approaches infinity. This condition is equivalent to $\mathrm{d}p/\mathrm{d}\xi = 0$ at $\xi = 0$ for any fixed time. Thus equation (31) is justified. The three coefficients a_1, a_2 and a_3 in equation (31) can be determined by the three values of z at the three trial values of ξ. In the deformation–flow coupled problem we expect that the pore pressure behaves the same as in the uncoupled problem. Hence equation (31)

can be utilized for extrapolation. The other physical quantities are intimately related to the pore pressure and can also be evaluated by extrapolation with equation (31).

TEST PROBLEMS

To investigate the accuracy of our finite element method, two test problems are considered. Since the analytical solutions for the deformation–flow coupled problems are not found, our comparison of the finite element solution with the analytical solution is restricted to the uncoupled case where the effect of deformation is ignored.

The first problem is a pressure diffusion problem in a long hollow cylinder with prescribed inner and outer pressures as shown in Figure 1. The analytical solution of the uncoupled problem is given in Appendix I. Both analytical and finite element solutions are shown in Figure 2. Note that in the analytical solution the applied pressure on the inner boundary is a step function of time. It jumps from zero to a certain constant value initially. However, in the numerical solution the step function is replaced by a linear function of time in the first time step. Therefore at early time there is a large difference between the two solutions. However, this difference reduces rapidly with increasing time.

The second problem is a pressure diffusion problem in an infinitely large medium with a finite conductivity fracture. The analytical solution of the uncoupled problem is given by Cinco-Ley *et al.*[4] In our finite element solution we deal with the problem of diffusion into a rectangular crack with an impermeable crack tip, which is identical to the problem studied by Cinco-Ley *et al.* Our numerical method is given in Appendix II. Different finite element lay-outs with variable mesh sizes are adopted in our computation. The finite element mesh is shown in Figure 3. The finite element solution for the pressure drop under constant production rate is compared with the

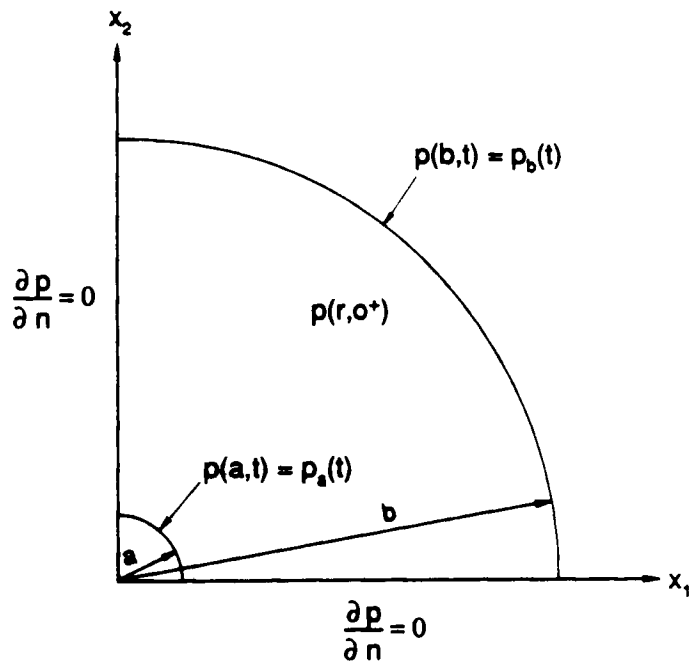

Figure 1. Geometry of the first test problem

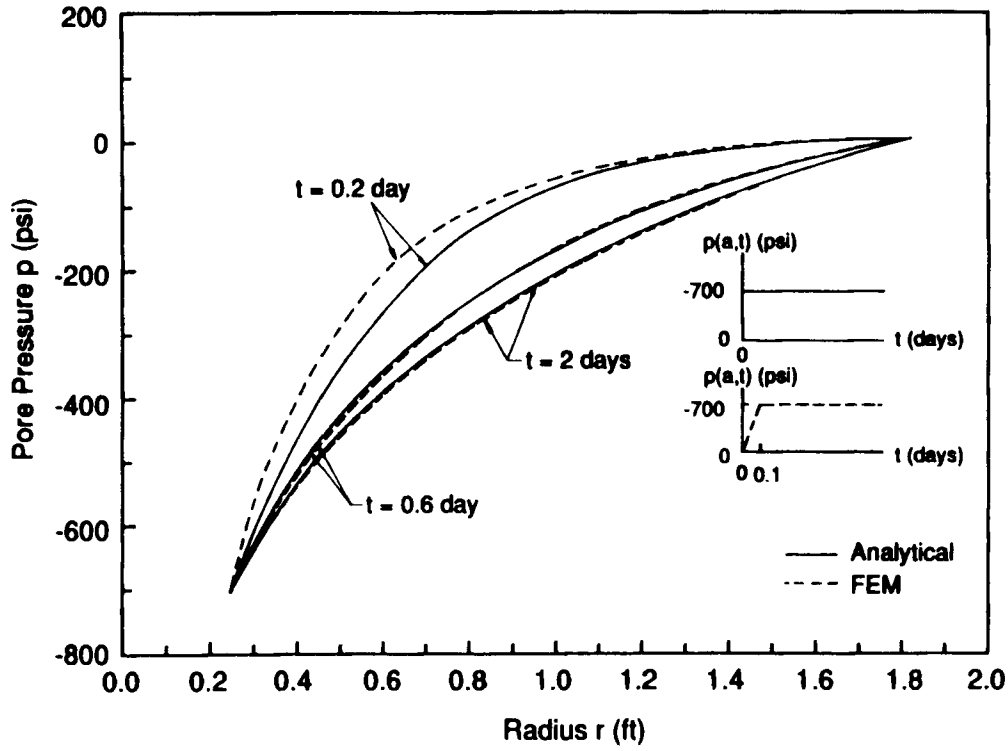

Figure 2. Comparison of the analytical solution of the pore pressure with the FEM solution in the first test problem

analytical solution in Figure 4. It is found that the pressure drop curves in these two solutions are essentially parallel. At early time the difference can be greater than 10%, but at later time the difference is less than 5%. The reason for the difference between Cinco-Ley *et al.*'s solution and the finite element solution can be explained as follows. (i) The analytical solution of Cinco-Ley *et al.* is also obtained numerically. A stepwise interpolation function for the flow flux density in the fracture in both space and time is applied. Hence the accuracy of their analytical solution depends on the numerical techniques. (ii) In the solution of Cinco-Ley *et al.* the prescribed production rate q_w is a step function of time. Such a step function of time cannot be generated in our finite element solution. It is replaced by a linear function of time in the first time step. Therefore a large difference between the two solutions exists at early time. However, it is found that the difference decreases with time. At large time the difference becomes so small that it does not have any engineering significance.

A SINGLE WELL IN AN INFINITE MEDIUM

Let us consider the problem of transient flow in the vicinity of a production well with radius r_w in an infinite isothermal medium. We assume that there exist initial confining stresses σ_{11}^{∞} and σ_{22}^{∞}, an initial pore pressure p_0 in the medium and a constant applied pressure p_i in the production well. The solution of this problem can be obtained by a superposition of two solutions of problems as shown in Figure 5. Solutions of stress field and pore pressure field in the first problem are a uniform stress field $\sigma_{11}=\sigma_{11}^{\infty}$, $\sigma_{22}=\sigma_{22}^{\infty}$ and $\sigma_{12}=0$ and a uniform pore pressure field $p=p_0$.

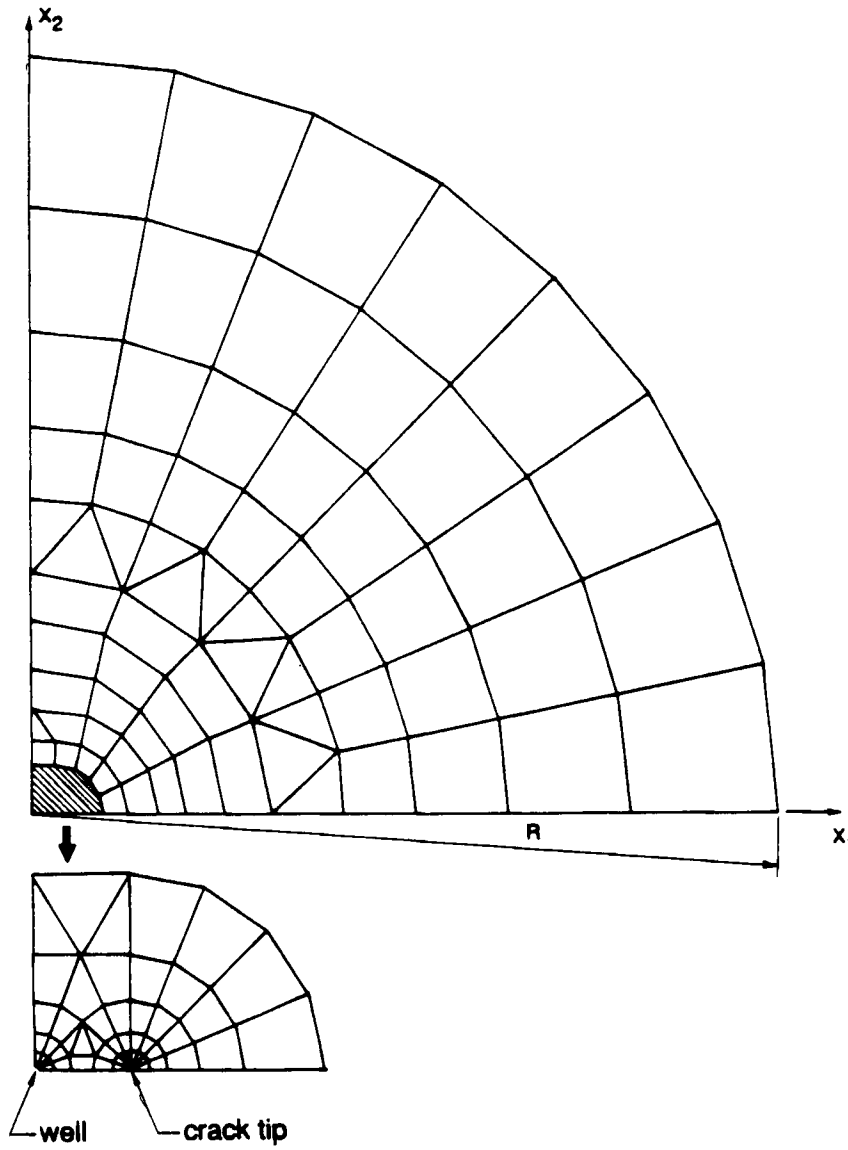

Figure 3. Finite element mesh of the conductive fracture problem

Solutions in the second problem will be obtained by the finite element method. The boundary conditions and initial conditions for the second problem are

$$P_1=(\sigma_{11}^{\infty}-p_i)\cos\theta \quad \text{and} \quad P_2=(\sigma_{22}^{\infty}-p_i)\sin\theta \quad \text{for } r=r_w, \tag{32}$$

$$u_1=u_2=0 \quad \text{for } r\to\infty, \tag{33}$$

$$p(r_w, t)=p_w=p_i-p_0 \quad \text{and} \quad p(\infty, t)=0 \quad \text{for } t>0, \tag{34}$$

$$p(r, 0)=0. \tag{35}$$

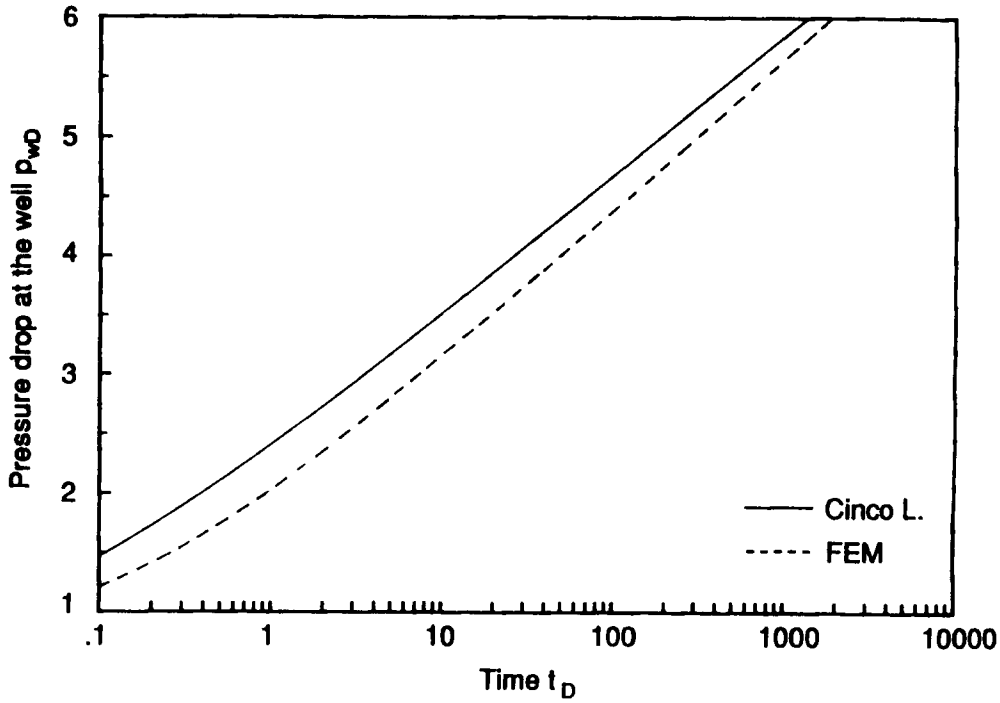

Figure 4. Comparison of the analytical solution in Reference 4 with the current FEM solution

As we have mentioned previously, owing to the diffusion of the pore pressure, our finite element solution at large time is inaccurate if we replace an infinite region by a finite region with the boundary conditions of equations (33) and (34) applied to the outer boundary. In this study a moderately large region will be used to replace the infinite medium. Since a direct employment of the boundary condition at infinity for the outer boundary of the finite region will cause a large error, the uncoupled solutions of pore pressure field in an infinite medium are used for the outer boundary conditions of the finite region. This approach is reasonable for the material point at a location far from the well, where the deformation of the medium is too small to have any influence on the pore pressure distribution.

For the case of uncoupled diffusion of pore pressure the governing differential equation for the pressure drop $p(r, t)$ in an axisymmetric region is a standard diffusion equation for the pressure in an axisymmetric region in the polar co-ordinate system. It is

$$\frac{\partial^2 p}{\partial r^2}+\frac{1}{r}\frac{\partial p}{\partial r}=\frac{1}{\eta}\frac{\partial p}{\partial t}, \tag{36}$$

where η is the diffusivity of the medium and is defined by $\eta = k/c$. With the use of the boundary condition, equation (34), and the initial condition, equation (35), the solution of equation (36) for any r is given by Jaeger[8] as

$$p(r, t)=p_w\left(1+\frac{2}{\pi}\int_0^\infty e^{-\tau u^2}\frac{J_0\left(u\frac{r}{r_w}\right)Y_0(u)-Y_0\left(u\frac{r}{r_w}\right)J_0(u)}{J_0^2(u)+Y_0^2(u)}\frac{du}{u}\right), \tag{37}$$

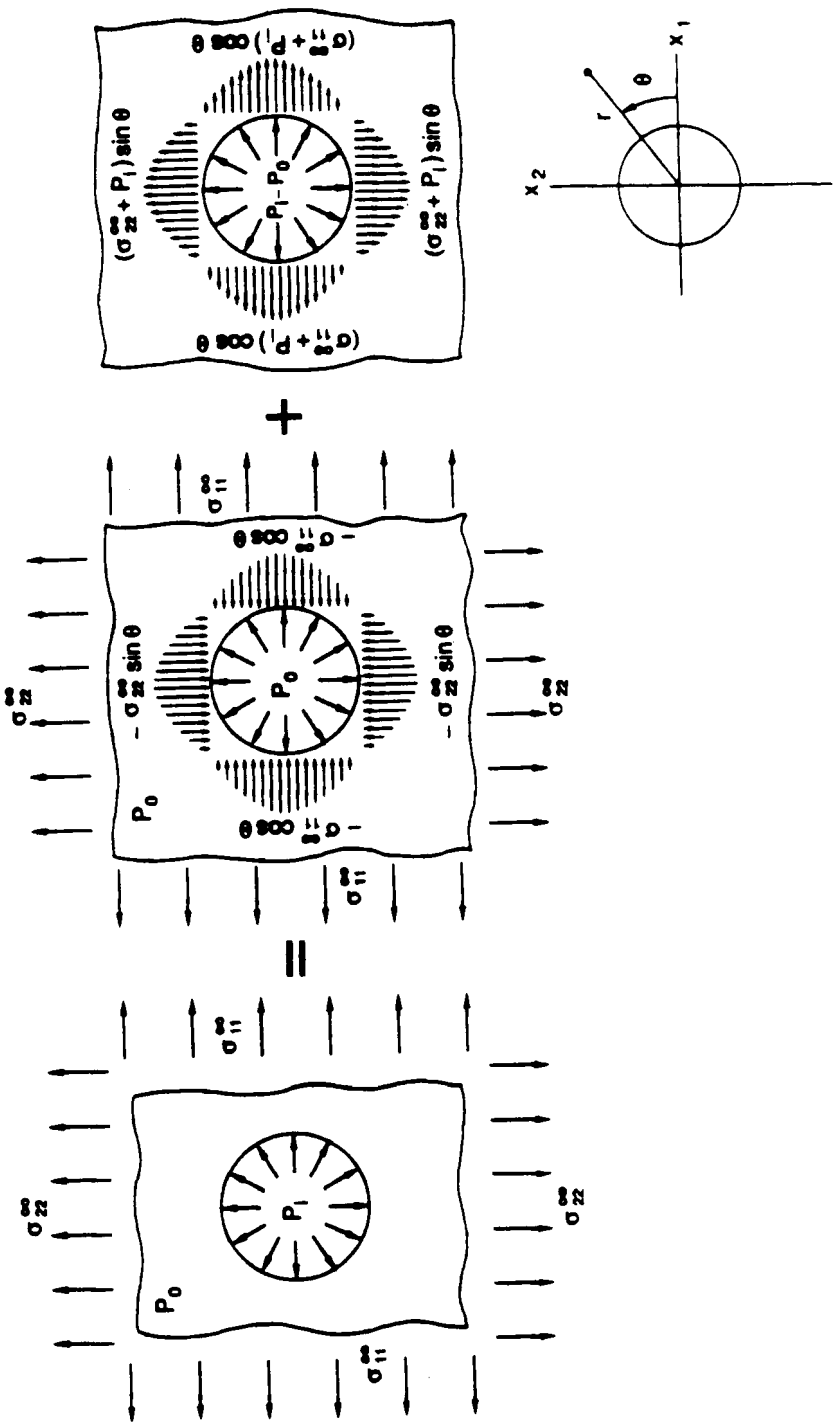

Figure 5. Illustration of the superposition method for the problem of a single well in an infinite medium without the conductive fracture

where J_0 and Y_0 are respectively the first and second kinds of Bessel functions of order zero and

$$\tau = \frac{\eta t}{r_w^2}. \tag{38}$$

As suggested by Jaeger, the range $(0, \infty)$ of the integral in equation (37) can be divided into two parts, $(0, 0{\cdot}2)$ and $(0{\cdot}2, \infty)$. The integral of the first part can be evaluated on the basis of an ascending series expression of the integrand, while the integral of the second part can be calculated directly.

A large annular domain with inner radius $r_w = 0{\cdot}25$ ft and outer radius $R = 180$ ft is considered in the finite element calculation. The confining stresses are $\sigma_{11}^{\infty} = -2000$ psi and $\sigma_{22}^{\infty} = -1500$ psi. The initial pore pressure is $p_0 = 800$ psi. The applied pressure in the production well is $p_i = 100$ psi. The physical constants are given as follows:

$$\begin{aligned} &\nu = 0{\cdot}15, \qquad \nu_p = \frac{\nu}{1-\nu} = 0{\cdot}1765, \qquad G = 1{\cdot}253 \times 10^8 \text{ psf}, \\ &\lambda_p = 0{\cdot}6372, \qquad c_p = 0{\cdot}34 \times 10^{-8} \text{ psf}^{-1}, \\ &K = 4{\cdot}453 \times 10^{-5} \text{ ft}^2 \text{ psf}^{-1} \text{ day}^{-1}, \qquad \eta = 13{\cdot}1 \times 10^3 \text{ ft}^2 \text{ day}^{-1}, \\ &k = 0{\cdot}2152 \times 10^{-14} \text{ ft}^2 = 0{\cdot}1957 \text{ md}, \qquad \phi = 0{\cdot}2, \qquad \mu = 0{\cdot}145 \times 10^{-6} \text{ psi s}, \end{aligned} \tag{39}$$

where the subscript 'p' denotes the case of plane strain. On the outer boundary $r = R$, pressures at different times are determined by equation (37) while the displacement is zero.

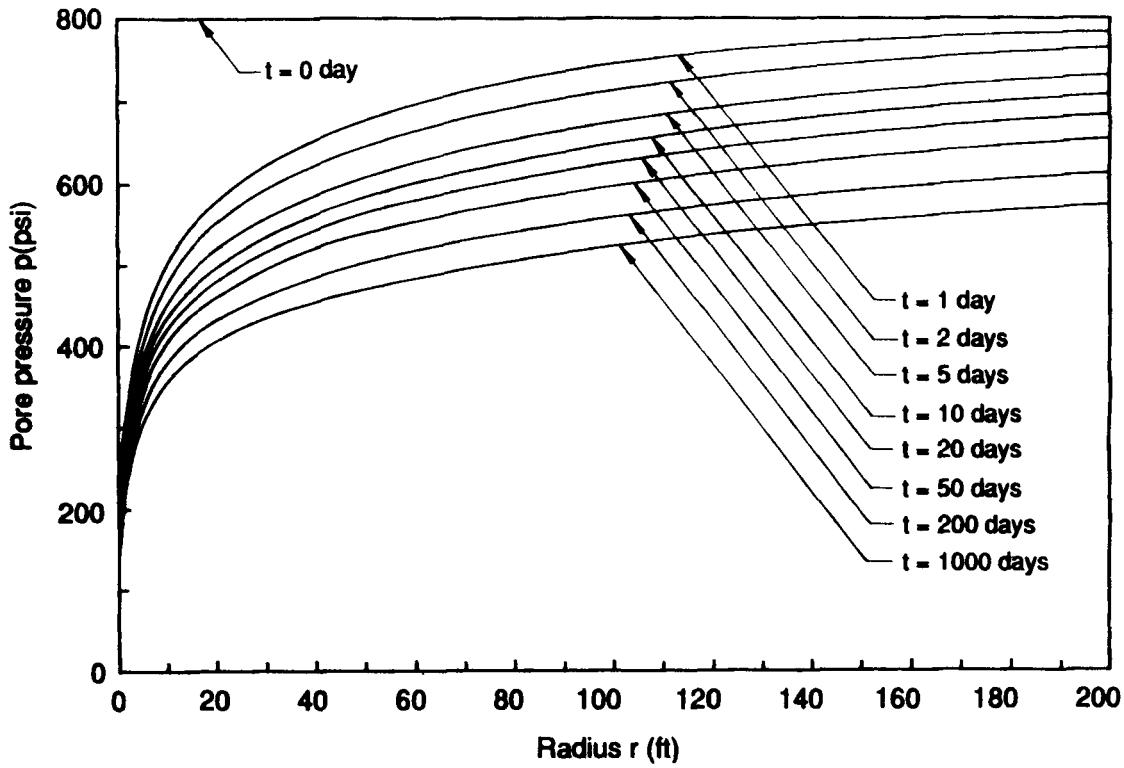

Figure 6. Distribution of the pore pressure in the infinite medium

The pore pressure distributions in the medium at different times are shown in Figure 6. It is seen that the pore pressure increases rapidly near the production well. At $t = 1000$ days the pore pressure at $r = 180$ ft is about 70% of the initial pressure. The distributions of the stress component $\sigma_\theta(r, 0)$ at $t = 0{\cdot}2$, 10 and 1000 days are shown in Figure 7. It is found that in the vicinity of the well the magnitude of $\sigma_\theta(r, 0)$ increases rapidly owing to the effect of stress concentration. At a location with a sufficiently large distance from the well the magnitude of the stress can be smaller than that of the confining stress σ_{22}^{∞}. However, in the region far from the well the stress approaches the confining stress asymptotically. Therefore hydraulic fracture can be generated near the well as the injected fluid is pumped into the well. Figure 8 shows that the production rate always decreases with increasing time and the rate of decrease becomes slow as time increases. After 5–10 years of production the production rate is only about 60% of the initial production rate.

Figure 9 shows the coupled and uncoupled solutions of the pore pressure in the medium. No noticeable difference between them is found. It is evident that in the case of a single well in an infinitely large medium, under our prescribed material constants, the deformation of oil formation has only negligible influence on the pore pressure distribution.

A FINITE CONDUCTIVITY FRACTURE IN AN INFINITELY LARGE MEDIUM

Let us consider a fully penetrating vertical fracture of length $2a$ with a well located at the centre. All material constants are given in equation (39). The *in situ* stresses and the initial pressure in the

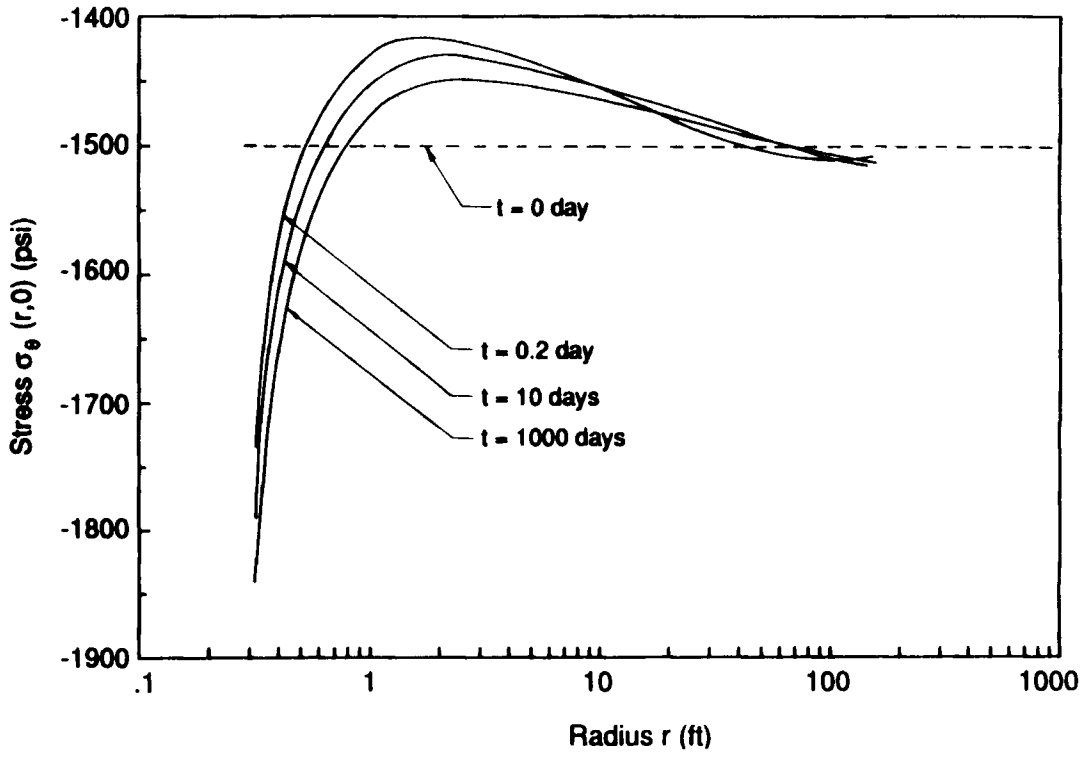

Figure 7. Distribution of the stress component $\sigma_\theta(r, 0)$ in the infinite medium

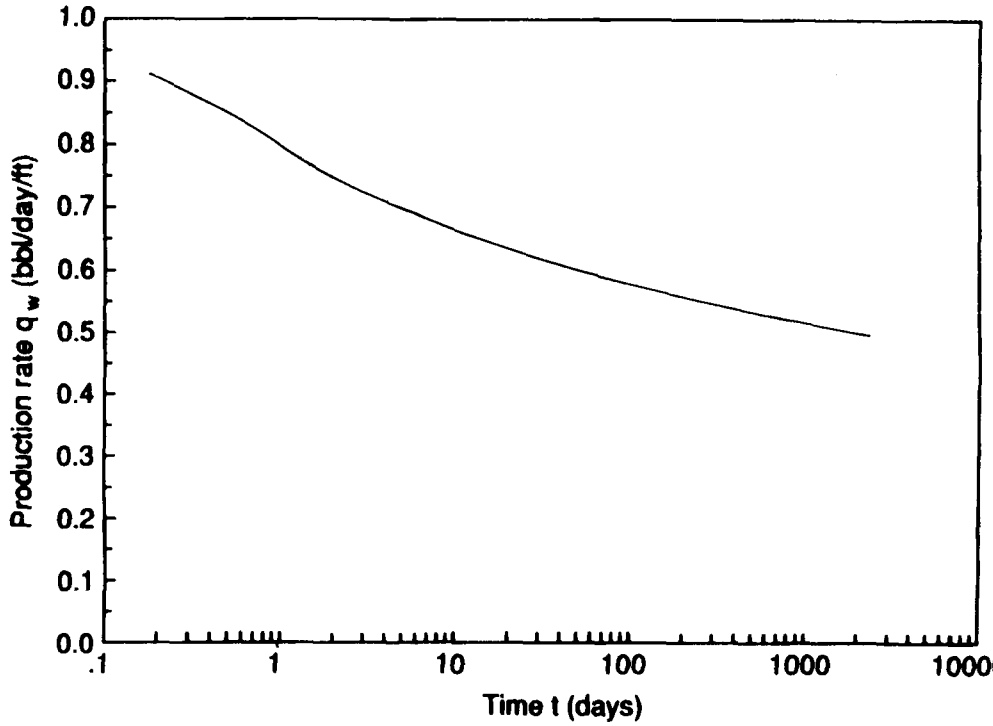

Figure 8. Curve of production rate q_w versus time t for the problem without the conductive fracture

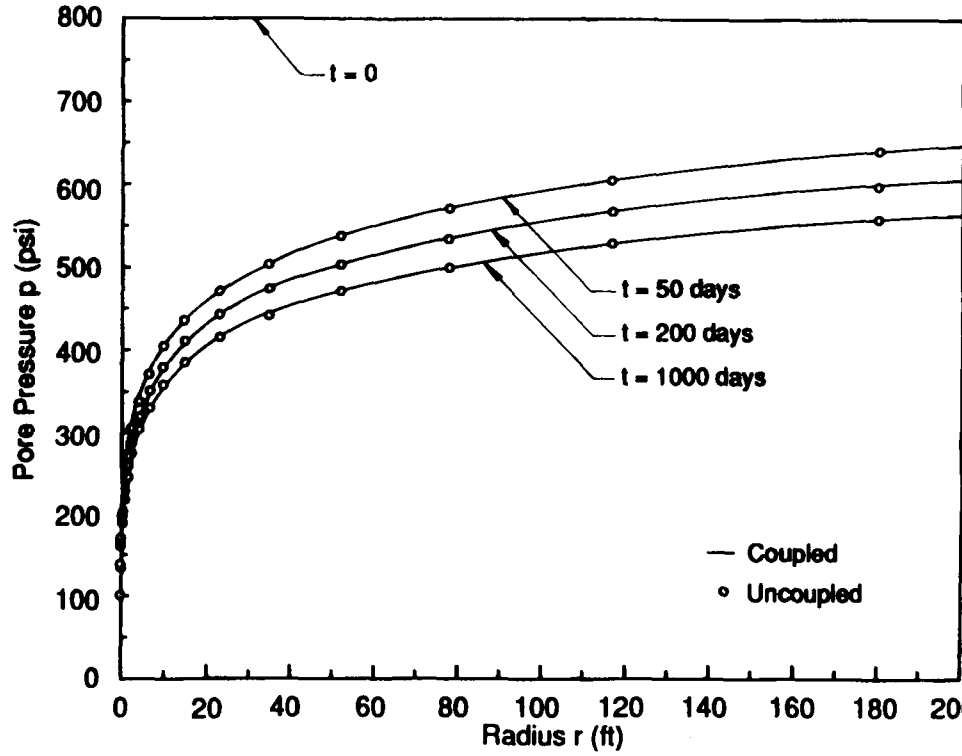

Figure 9. Comparison of coupled and uncoupled solutions of pressure distribution

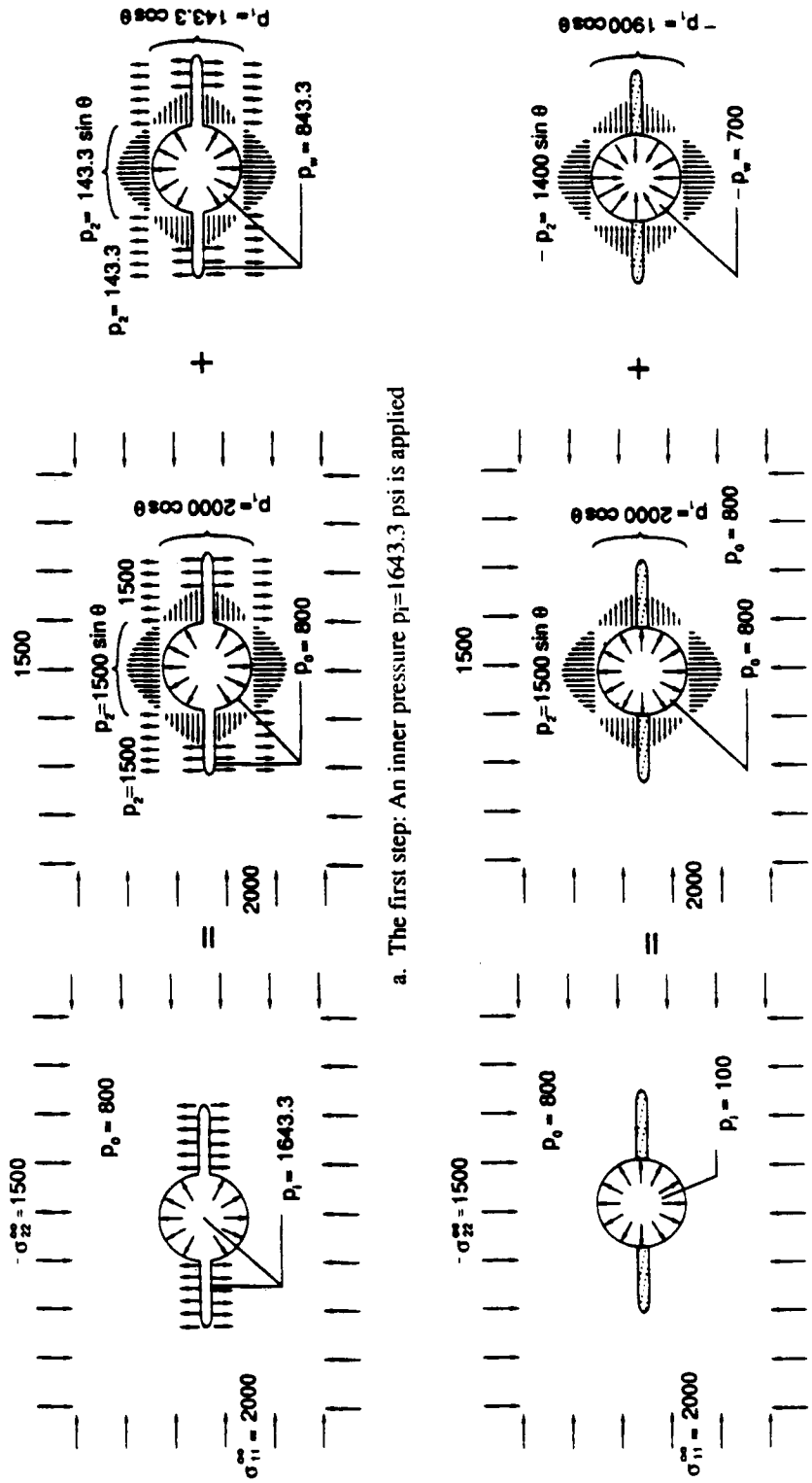

a. The first step: An inner pressure p_i=1643.3 psi is applied

b. The second step: The applied pressure p_i drops to 100 psi

Figure 10. Illustration of the superposition method for the problem of a single well in an infinite medium with a conductive fracture

reservoir are the same as those used in the previous problem. The pressure applied to the well exceeds the *in situ* stress σ_{22}^{∞} by 143·3 psi, generating a crack with a crack-mouth-opening displacement of $\frac{1}{3}$ inch at the well-bore. As it drops to 100 psi afterwards, the opened crack is retained by the sand in the fracture. This procedure of crack opening and sand filling is completed in such a short time that we may consider that it takes place instantly. Thus we have an initial value problem. It consists of two steps as shown in Figure 10. In the first step (Figure 10a) an inner pressure $p_i = 1643{\cdot}3$ psi is applied to the crack surface and the wall of the well. This step can be regarded as a superposition of two problems. The first problem has the solution of a uniform stress field $\sigma_{11} = -2000$ psi, $\sigma_{22} = -1500$ psi and $\sigma_{12} = 0$ and a uniform pore pressure field $p = 800$ psi. In the second problem the pore pressure is zero everywhere except at the crack surface and the well wall, where the pore pressure is 843·3 psi. The deformation in the second problem can be obtained by the finite element method. In the second step (Figure 10b) the applied inner pressure drops to 100 psi and the crack is filled with sand. This step can also be divided into two problems. Although the geometry and loading condition are different from those in the first step, the solution of the first problem of the second step still gives uniform fields of stress and pore pressure which are the same as in the first step. In this analysis the solution of the second problem of the first step is used as the initial condition of the second problem of the second step. The final solution of the second step can be obtained by superposition of these two problems.

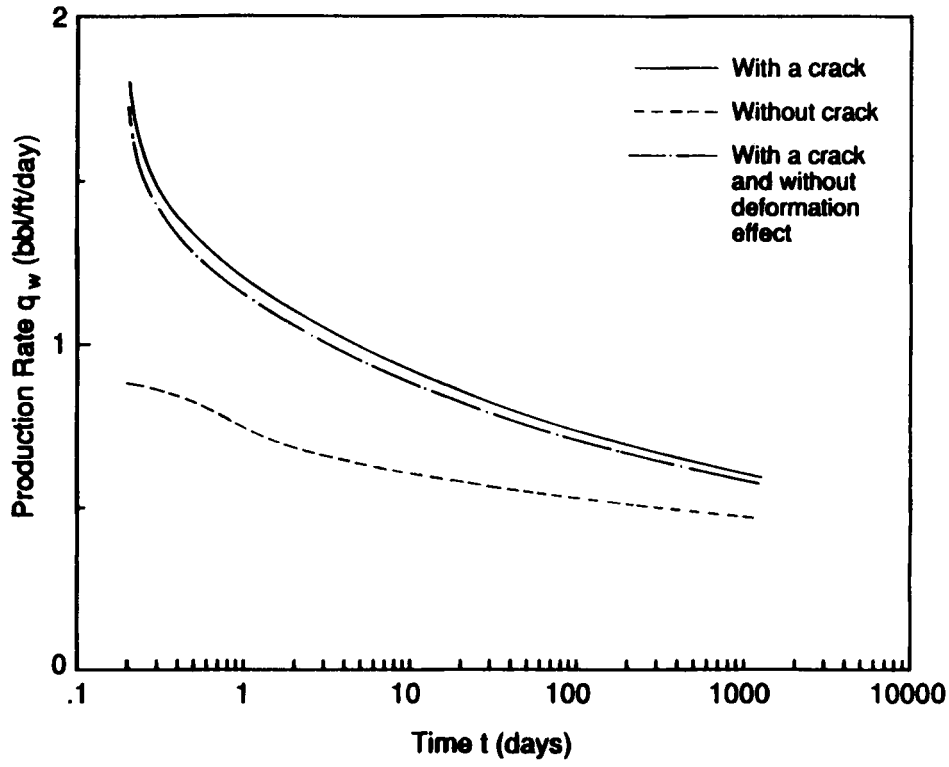

Figure 11. Curves of production rate q_w versus time t for the problem with a conductive fracture

The following material and geometrical constants of the conductive fracture are employed in our computation:

$$K_f = 0{\cdot}044\,53\ \text{ft}^2\ \text{psf}^{-1}\ \text{day}^{-1}, \qquad \lambda_f = 0{\cdot}5012, \qquad c_f = 0{\cdot}225 \times 10^{-8}\ \text{psf}^{-1},$$
$$E_f = 0{\cdot}1566 \times 10^9\ \text{psf}, \qquad k_f = 0{\cdot}2152 \times 10^{-11}\ \text{ft}^2 = 195{\cdot}7\ \text{md},$$
$$\phi_f = 0{\cdot}2, \qquad \mu_f = 0{\cdot}145 \times 10^{-6}\ \text{psi s}, \qquad a = 100\ \text{ft}. \tag{40}$$

The finite element mesh is shown in Figure 3. The numerical results are shown in Figures 11–21. Figure 11 shows that the production rate q_w decreases with increasing time for a prescribed constant applied pressure. At early time the production rate is about twice that without the conductive crack. Even at $t = 1000$ days the former is still about 1·2 times as large as the latter. It is found that nearly 96% of the production rate stems from the conductive crack. The pore pressure distributions on the x_1- and x_2-axes are shown in Figures 12–14, which indicate that the pore pressure approaches its initial value p_0 when the location is further from the well. Figures 15–18 show the distributions of stresses σ_{11} and σ_{22} on the x_1- and x_2-axes, where the effect of stress concentration at the crack tip and on the wall of the well can be seen. The stresses approach the *in situ* stresses when x_1 and x_2 approach infinity. As a result of decreasing pore pressure with time, the load transfers to the skeleton and the magnitude of stresses increases with time. Figures 19 and 20 show the distributions of displacement u_1 on the x_1-axis and displacement u_2 on the x_2-axis. At early time both u_1 and u_2 are approximately zero near the well. At later time, as a result of the diffusion of the pore pressure, these displacements have large values in large ranges

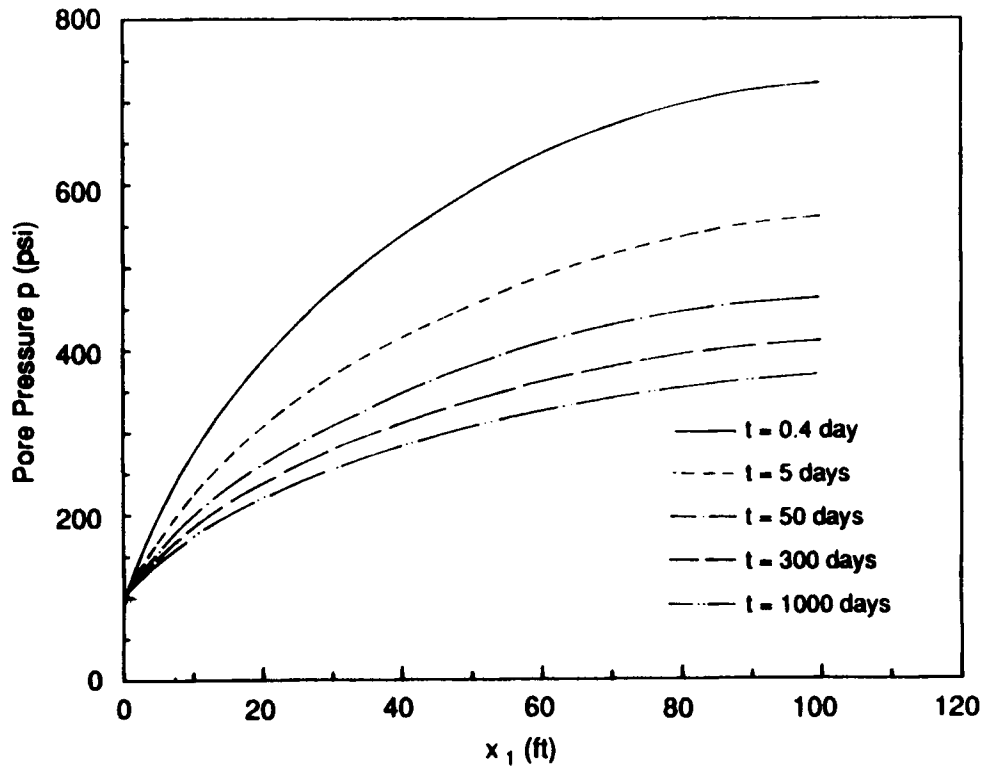

Figure 12. Distribution of the pore pressure p on the crack surface

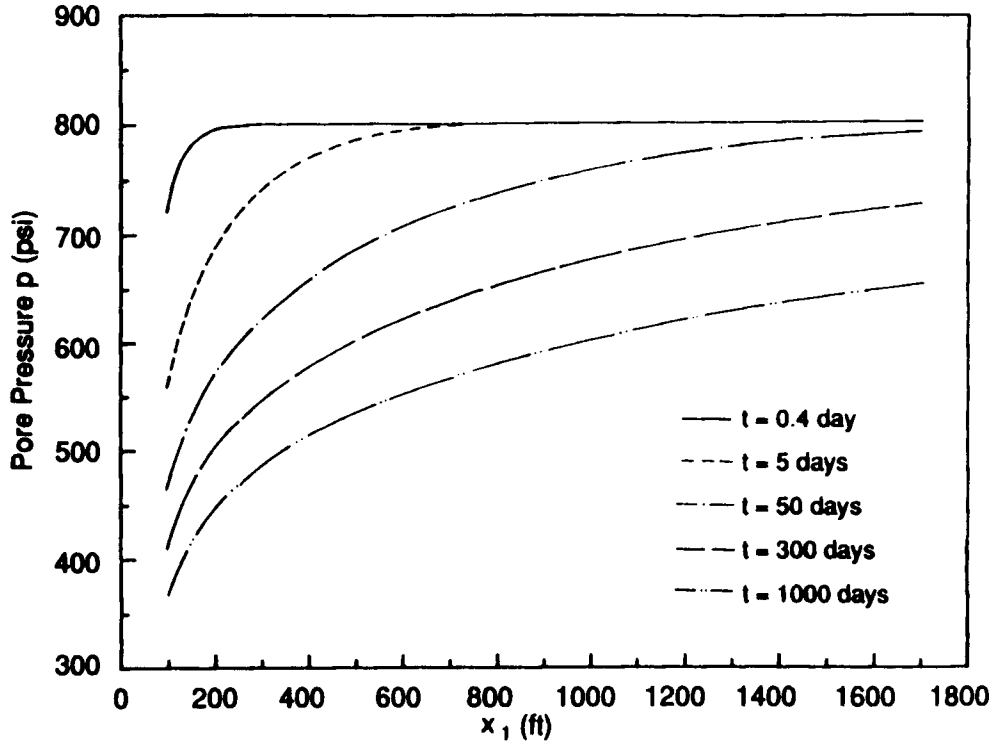

Figure 13. Distribution of the pore pressure p on the x_1-axis

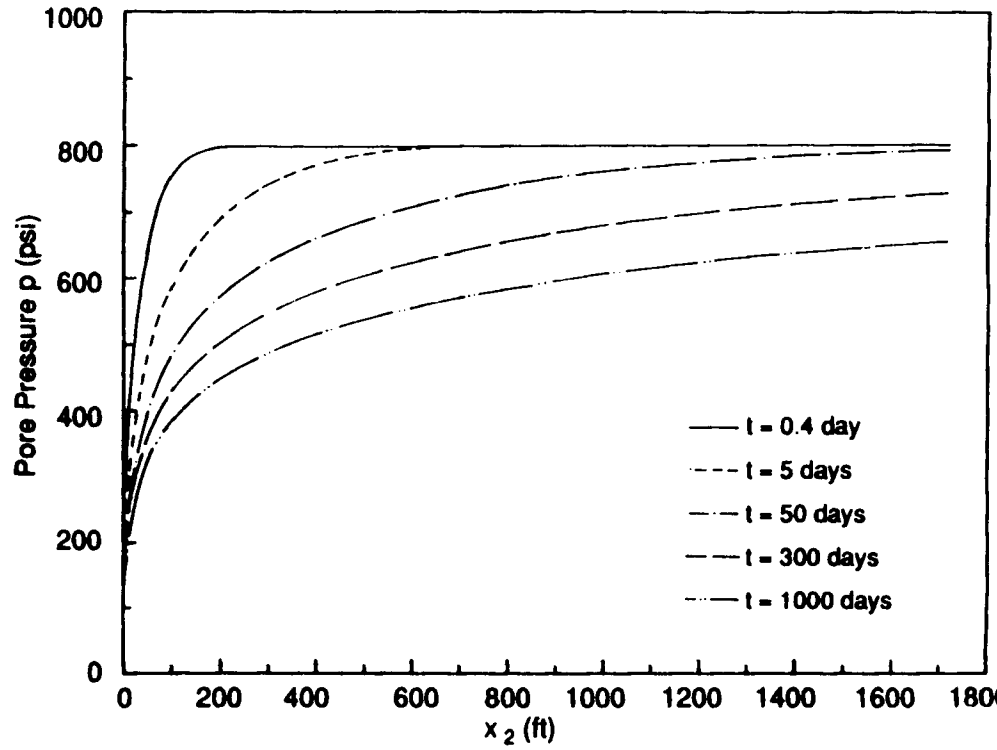

Figure 14. Distribution of the pore pressure p on the x_2-axis

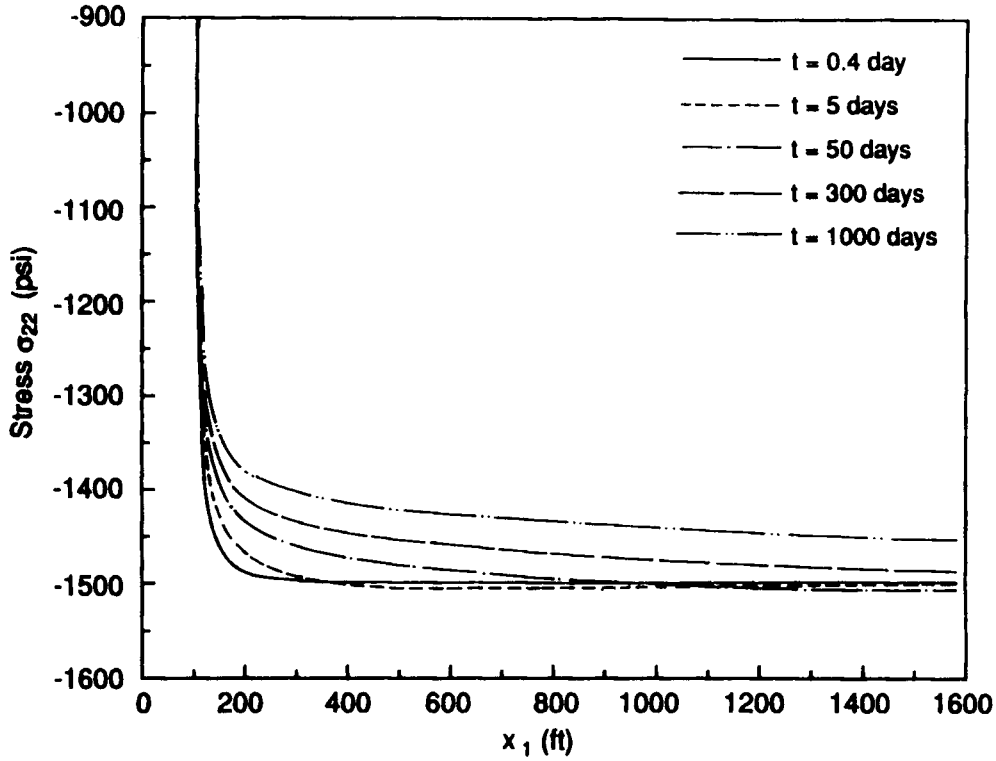

Figure 15. Distribution of the stress component σ_{22} on the x_1-axis

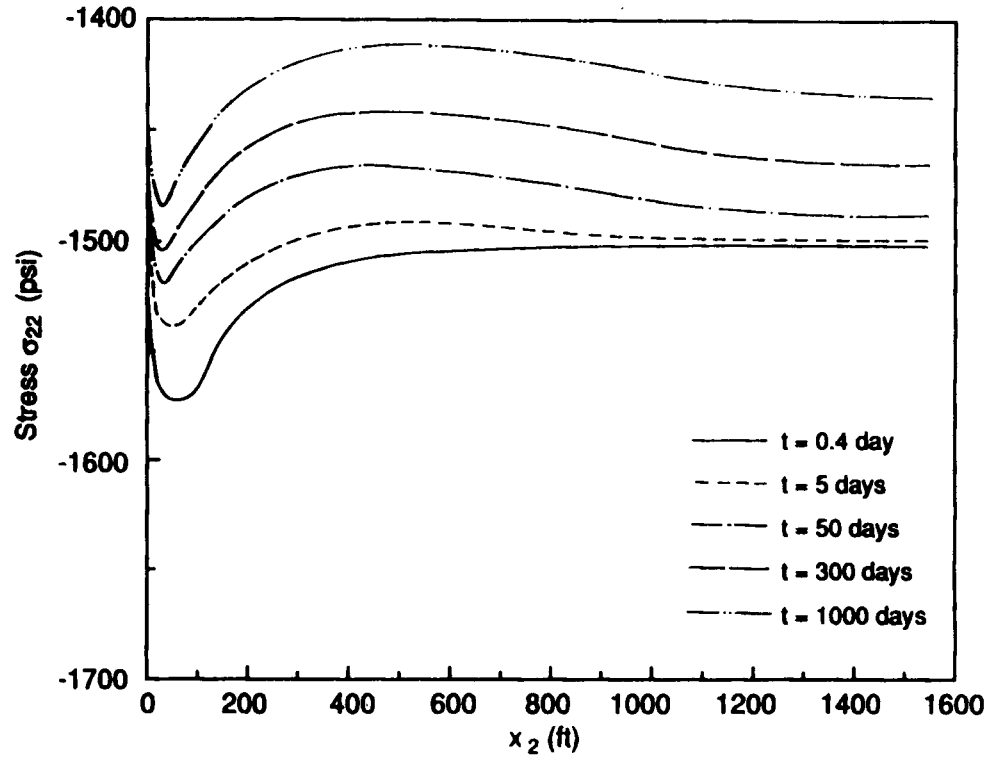

Figure 16. Distribution of the stress component σ_{22} on the x_2-axis

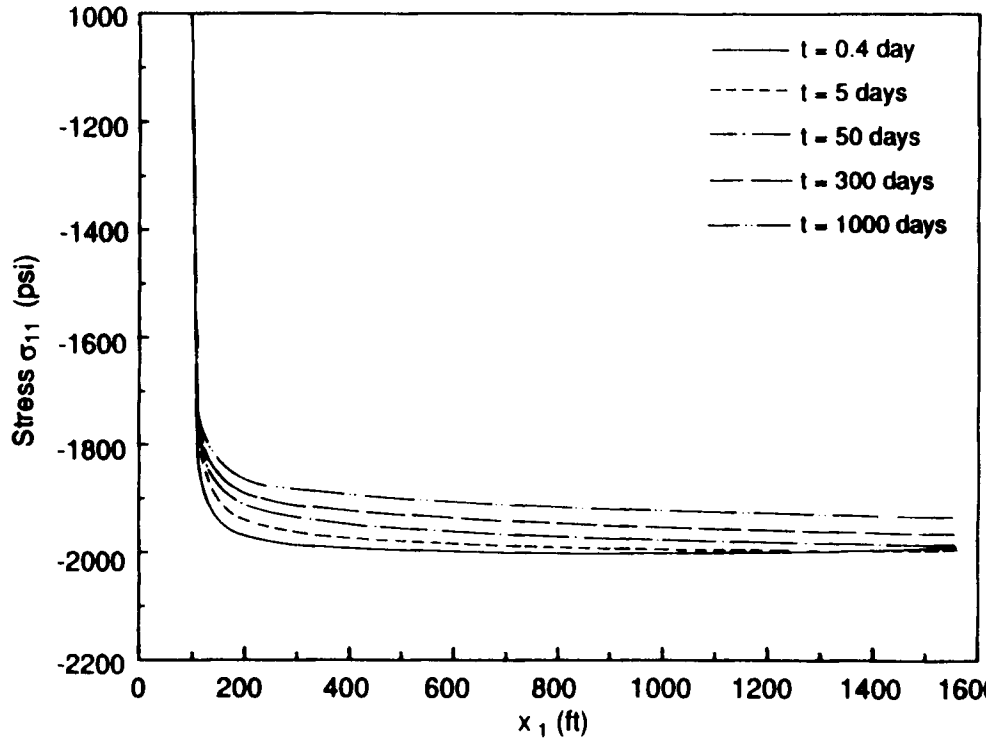

Figure 17. Distribution of the stress component σ_{11} on the x_1-axis

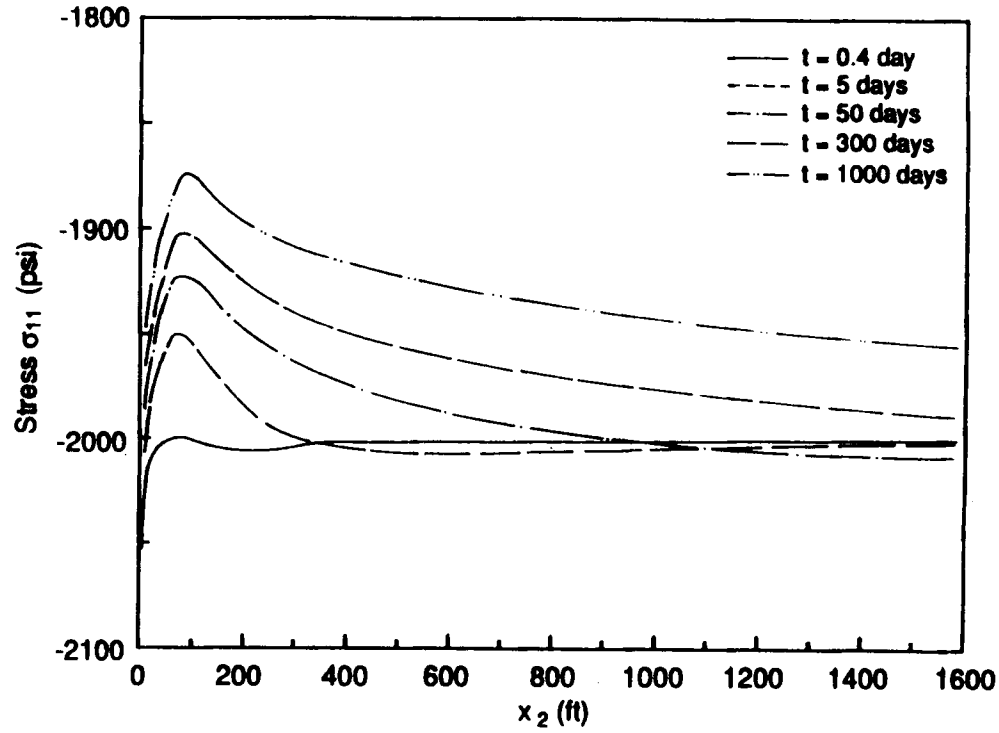

Figure 18. Distribution of the stress component σ_{11} on the x_2-axis

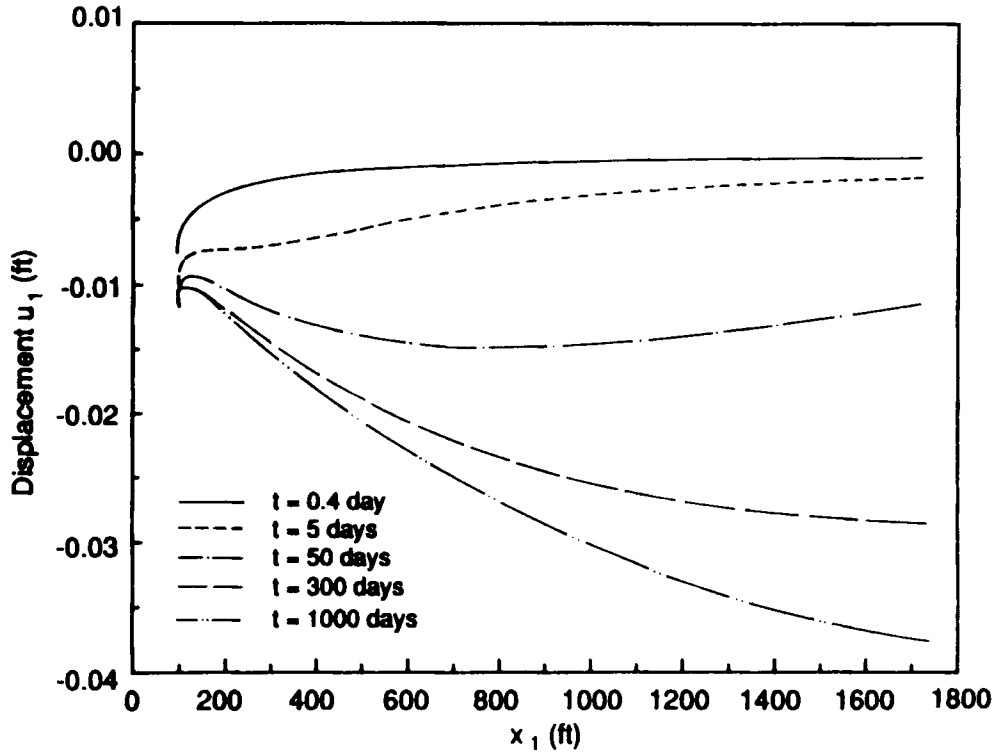

Figure 19. Distribution of the displacement component u_1 on the x_1-axis

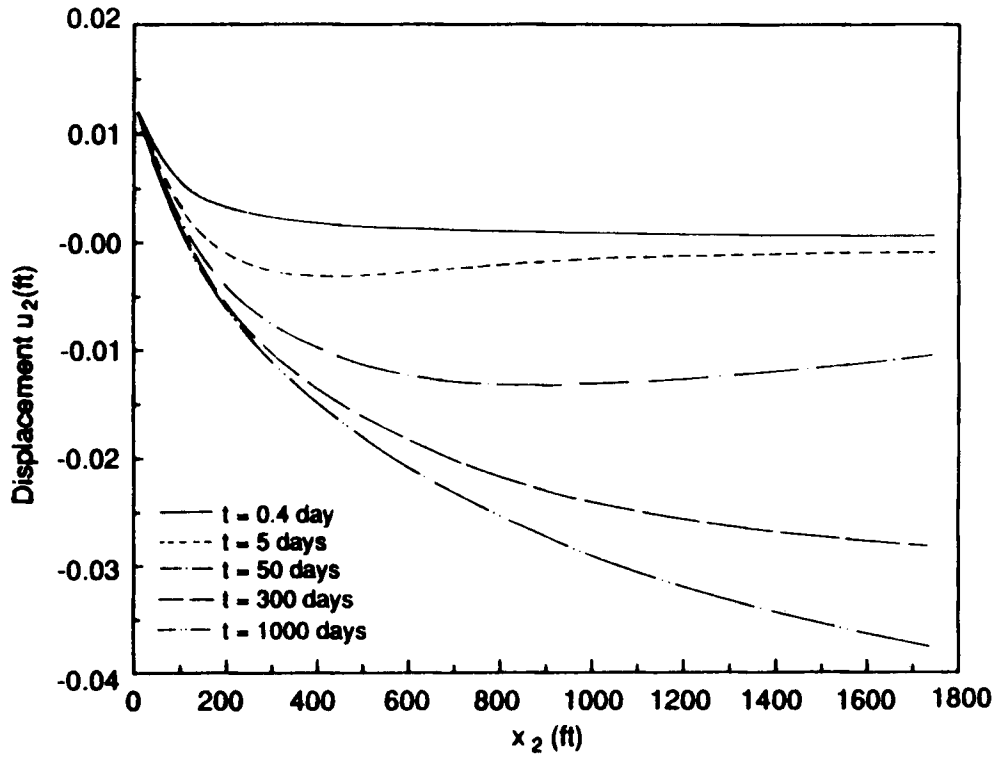

Figure 20. Distribution of the displacement component u_2 on the x_2-axis

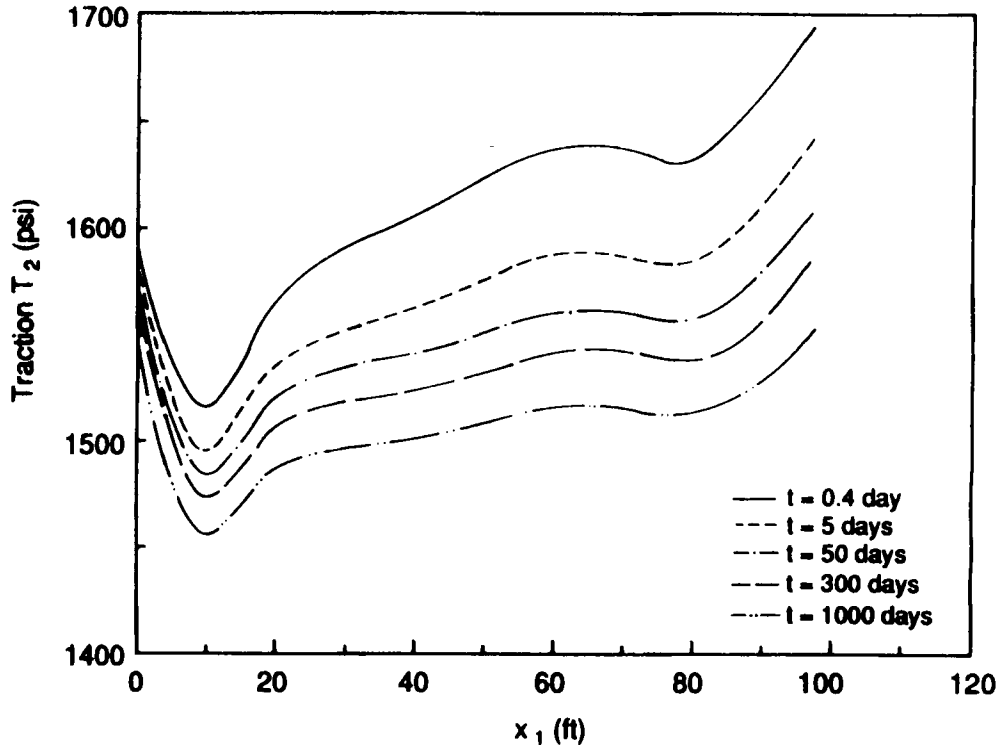

Figure 21. Distribution of the traction T_2 on the crack surface

of x_1 and x_2. In the calculation it is found that the crack profile has only a small difference from the initial crack profile, although the transverse strain ε_{22} in the crack and the traction T_2 are large. Figure 21 shows the distribution of the traction T_2 on the crack surface, where the effect of stress concentration is seen on the wall of the well. This traction must maintain at a certain level in order to prevent the sand from flowing with the liquid.

If the poroelastic constants λ and λ_f are set to zero, our problem degenerates to an uncoupled pure diffusion problem. The production rate is also shown in Figure 11 and is compared with that of the coupled problem. Differences of nearly 4% at early time and 10% at later time are found.

CONCLUSIONS

In this study the variational principle of Huang *et al.*[6] is applied to develop a finite element method for analysing transient deformation–pore pressure coupled problems for wells with/without finite conductivity vertical fractures. Comparison of the numerical results with theoretical results demonstrates the accuracy and reliability of the method. The following conclusions can be drawn from our study.

1. For non-zero *in situ* stress and initial pore pressure fields the problem can be resolved into two problems. One of them has the solution of uniform stress and pore pressure fields. The other can be solved by means of the finite element method. The real solution of the problem can be obtained by superposition of these two problems.
2. For the problem of a well in an infinite region without the conductive crack the infinite region can be replaced by a finite large annular region with the centre at the well. The

boundary condition on the outer boundary of the annular region can be determined by the analytical solution for transient pressure behaviour in the infinite region of an uncoupled problem. The computational results demonstrate that there is no noticeable difference between the transient pressure behaviour and the coupled transient deformation–pressure behaviour.

3. For the problem of a well in an infinite region with a finite conductivity crack our investigation presents a realistic model and demonstrates a powerful technique. We first obtain the solution for finite large regions. The outer boundary of the region in each solution is a circle of radius R concentric with the well. The solution for the infinite region can be determined by the limiting case of $1/R^2$ approaching zero, which is computed by extrapolation of the solutions for finite regions with different values of $1/R^2$. Our computational results indicate that the extrapolation is well behaved. The extrapolation function has zero slope at $1/R^2=0$.
4. Our analysis indicates that the conductive crack plays an important role in increasing the oil production rate. Most oil production is derived from the conductive crack.
5. Our investigation demonstrates that for the conductive crack problem there is only a small difference in oil production rate between the transient pressure problem and the coupled transient deformation–pressure problem for a prescribed constant applied pressure at the well. However, with different physical constants the picture may change. For large values of the poroelasticity constants λ and λ_f, the difference between the coupled and uncoupled solutions can become noticeable.

ACKNOWLEDGEMENTS

The authors gratefully thank Dr. Jacob Shlyapobersky for his valuable discussion.

This work is sponsored by research grants-A-88-12-00013 from Shell Development Company and 88-25-1-ART0205 from Amoco Production Company with the University of Notre Dame.

APPENDIX I: PRESSURE DIFFUSION PROBLEM IN A HOLLOW CYLINDER

Let us consider the problem of axisymmetrical and uncoupled pressure diffusion in a long cylindrical region. Denote the inner radius of the cylinder by a, the outer radius by b, the inner pressure by p_a and the outer pressure by p_b. The analytical solution is found in Reference 9 as

$$p(r,t)=-\pi\sum_{n=1}^{\infty}\frac{[p_b J_0(a\alpha_n)-p_a J_0(b\alpha_n)]J_0(a\alpha_n)}{J_0^2(a\alpha_n)-J_0^2(b\alpha_n)}[J_0(r\alpha_n)Y_0(b\alpha_n)-J_0(b\alpha_n)Y_0(r\alpha_n)]e^{-\eta\alpha_n^2 t}$$
$$+\frac{p_a\ln(b/r)+p_b\ln(r/a)}{\ln(b/a)}, \tag{41}$$

where α_n $(n=1, 2, \ldots)$ are the roots of the equation

$$J_0(a\alpha)Y_0(b\alpha)-J_0(b\alpha)Y_0(a\alpha)=0. \tag{42}$$

The diffusivity coefficient is

$$\eta=K/c. \tag{43}$$

The problem is also solved by the finite element method. Because of axisymmetry, only the first quadrant needs to be considered. The element mesh consists of a set of concentric circles. There are eight element layers in the radial direction of the domain. Each layer includes four isoparametric elements. There are 32 elements and 45 nodal points in total. On the boundaries

$x_1=0$ and $x_2=0$ the normal gradient of the pore pressure is zero as a result of axisymmetry (Figure 1). The diffusivity coefficient, the size of the hollow cylinder, the boundary conditions and the initial conditions are prescribed as

$$\eta=0{\cdot}8434\ \text{ft}^2\ \text{day}^{-1}, \tag{44}$$

$$a=0{\cdot}25\ \text{ft}, \qquad b=1{\cdot}8\ \text{ft}, \tag{45}$$

$$p_a(t)=-700\ \text{psi} \quad \text{and} \quad p_b(t)=0 \quad \text{for } t>0, \tag{46}$$

$$p(r,0)=0. \tag{47}$$

The aforementioned computational scheme is used for the problem. The time increment $\Delta t=0{\cdot}1$ day is chosen in the calculation. Both numerical and analytical results of the pore pressure are shown in Figure 2.

APPENDIX II: TRANSIENT PRESSURE BEHAVIOUR FOR A FINITE CONDUCTIVITY FRACTURE

The governing differential equation in the reservoir is a typical diffusion equation, which is

$$p_{,ii}=\frac{1}{\eta}\dot{p}. \tag{48}$$

In the conductive fracture the governing equation is

$$b_f K_f p_{,ii}=b_f c_f \dot{p}+2v_n, \tag{49}$$

where b_f is the width of the conductive crack. On the crack surface and at the crack tip the pressure and flow velocity are continuous. Thus the leak-off velocity can be expressed by

$$v_n=-K\frac{\partial p(x_1,0;t)}{\partial x_2} \quad \text{for } r_w<x_1<a. \tag{50}$$

Let us consider a finite large circle of radius R concentric with the well. A finite rectangular crack is extended from the well-bore and located on the x_1-axis from $x_1=-a$ to $x_1=a$ with a width b_f and an impermeable crack tip. Because of the symmetry in geometry, only the first quadrant of the circle needs to be considered. Assuming (i) a prescribed constant flow rate per unit height of the formation q_w in the production well, (ii) an impermeable well wall and (iii) zero pressure on the outer boundary of the region, the boundary condition of the reservoir can be written as

$$\frac{\partial p(0,x_2;t)}{\partial x_1}=0 \quad \text{for } x_2\geq r_w, \tag{51}$$

$$\frac{\partial p(x_1,0;t)}{\partial x_2}=0 \quad \text{for } x_1\geq a, \tag{52}$$

$$p(x_1,x_2;t)=0 \quad \text{for } r=R, \tag{53}$$

$$\frac{\partial p(x_1,x_2;t)}{\partial n}=0 \quad \text{for } r=r_w \text{ (except at the opened crack mouth).} \tag{54}$$

The initial condition is

$$p(x_1,x_2;0)=0. \tag{55}$$

Table I. Main parameters of the finite element mesh

Radius of domain R (ft)	Number of elements	Number of nodes
3125	128	141
3906	136	150
4883	144	159

For the conductive fracture the boundary conditions are

$$\frac{\partial}{\partial x_1} p(a, t)=0, \qquad -2K_f b_f \frac{\partial}{\partial x_1} p(0, t)=q_w, \tag{56}$$

which are also used by Cinco-Ley *et al.*[4] Under these assumptions and conditions our problem is the same as that of Cinco-Ley *et al.*

In order to compare our finite element solution with the solution of Cinco-Ley *et al.*, we introduce the following dimensionless quantities and parameters as given in their analysis:

$$p_D=(2\pi K/q_w)(p_0-p), \qquad x_{iD}=x_i/a, \qquad t_D=(\eta/a^2)t, \tag{57}$$

$$F_D=k_f b_f/(ka), \tag{58}$$

$$\eta_{fD}=\eta_f/\eta, \tag{59}$$

where p_D is the dimensionless pressure drop, F_D is the dimensionless fracture conductivity and η_{fD} is the dimensionless fracture diffusivity. The subscript 'D' refers to the dimensionless quantities. Note that the dimensionless quantities p_D and t_D in equation (57) are the same as those used by Cinco-Ley *et al.* Constant multipliers are introduced in Cinco-Ley *et al.*'s non-dimensional quantities for the purpose of conversion of units.

The finite element mesh for a large finite domain is shown in Figure 3. In the vicinity of the crack tip and the well a spider's-web-shaped mesh is used. The solution for an infinitely large domain can be obtained by the aforementioned extrapolation method. In our algorithm three values of the radius R of the outer boundary of the domain are considered. The corresponding element and node numbers are shown in Table I.

The dimensionless pressure drops in the well, p_{wD}, in both our finite element solution and Cinco-Ley *et al.*'s analytical solution are computed for $F_D=0{\cdot}2\pi$ and $\eta_{fD}=\infty$ ($c_f=0$, i.e. for the case of incompressible flow in the fracture). The material constants K, k and η for the porous medium given in (39) and k_f for the conductive crack in (40) are employed in the calculation. Note that the crack width b_f is not an independent quantity. It has to be determined by equation (57) for prescribed values of F_D, K_f, K and a. The results for p_{wD} of our finite element solution are evaluated as a function of the dimensionless time t_D. Our finite element solution is compared with Cinco-Ley *et al.*'s analytical solution[4] in Figure 4.

REFERENCES

1. A. C. Gringarten, H. J. Ramey and R. Raghavan, 'Unsteady state pressure distributions created by a well with a single infinite conductivity vertical fracture', *Soc. Petrol. Eng. J.*, 347–360 (August 1974).
2. F. Kucuk, *Ph.D. Thesis*, Stanford University, 1978.
3. F. Kucuk and W. E. Brigham, 'Transient flow in elliptic systems', *Soc. Petrol. Eng. J.*, 401–410 (December 1979).
4. H. Cinco-Ley, V. F. Samaniego and N. Dominguez, 'Transient pressure analysis for a well with finite conductivity fracture', *Soc. Petrol. Eng. J.*, 253–264 (August 1978).

5. M. A. Biot, 'General theory of three-dimensional consolidation', *J. Appl. Phys.*, **12**, 155–164 (1941).
6. N. C. Huang, A. A. Szewczyk and Y. C. Li, 'Variational principles and finite element method for stress analysis of porous media', *Int. j. anal. numer. methods geomech.*, **14**, 1–26 (1990).
7. J. R. Rice and D. M. Tracey, 'Computational fracture mechanics', in S. J. Fenves, N. Perrone, A. R. Robinson and W. C. Schnobrich (eds), *Numerical and Computer Methods in Structural Mechanics*, Academic, New York, 1977, pp. 533–536.
8. J. C. Jaeger, 'Numerical values for the temperature in radial heat flow', *J. Math. Phys.*, **34**, 316–321 (1955).
9. H. S. Carslaw and J. C. Jaeger, *Conduction of Heat in Solids*, 2nd edn, Clarendon, Oxford, 1959, pp. 205–208.